Journal of Materials Chemistry A

Localized Heating by a Photothermal Polydopamine Coating Facilitates a Novel Membrane Distillation Process

Journal:	*Journal of Materials Chemistry A*
Manuscript ID	TA-COM-06-2018-005738.R1
Article Type:	Communication
Date Submitted by the Author:	02-Aug-2018
Complete List of Authors:	Wu, Xuanhao; Washington University in St. Louis, Department of Energy, Environmental and Chemical Engineering Jiang, Qisheng; Washington University in St. Louis, Department of Mechanical Engineering and Materials Science Ghim, Deoukchen; Washington University in St. Louis, Department of Energy, Environmental and Chemical Engineering Singamaneni, Srikanth; Washington University in St. Louis, Department of Mechanical Engineering and Materials Science Jun, Young-Shin; Washington University in St. Louis, Department of Energy, Environmental and Chemical Engineering

Localized Heating by a Photothermal Polydopamine Coating Facilitates a Novel Membrane Distillation Process

Xuanhao Wu[1], Qisheng Jiang[2], Deoukchen Ghim[1], Srikanth Singamaneni[2, *] and Young-Shin Jun[1, *]

[1]*Department of Energy, Environmental and Chemical Engineering, Washington University in St. Louis, St. Louis, Missouri, 63130, USA. E-mail: ysjun@seas.wustl.edu*

[2]*Department of Mechanical Engineering and Materials Science, Washington University in St. Louis, St. Louis, Missouri, 63130, USA. E-mail: singamaneni@wustl.edu*

Submitted: August 2018

Journal of Materials Chemistry A

*To Whom Correspondence Should be Addressed

ABSTRACT

Solar-driven membrane distillation using photothermal membranes is of considerable interest for future water desalination systems. However, the low energy efficiency, complex synthesis, and instability of current photothermal materials hinder their further development and practicability. In this study, for the first time, we demonstrate a simple, stable, and scalable polydopamine (PDA) coated polyvinylidene fluoride (PVDF) membrane for highly efficient solar-driven membrane distillation. Our membrane shows the best energy efficiency among existing photothermal membranes (45%), and the highest water flux (0.49 $kg/m^2 \cdot h$) using a direct contact membrane distillation (DCMD) system under 0.75 kW/m^2 solar irradiation. Such performance was facilitated by the PDA coating, whose broad light absorption and outstanding photothermal conversion properties enable higher transmembrane temperature and increased driving force for vapor transport. In addition, the excellent hydrophobicity achieved by fluoro-silanization gives the membrane great wetting resistance and high salt rejection. More importantly, the robustness of our membrane, stemming from the excellent underwater adhesion of the PDA, makes the composite membrane an outstanding candidate for real-world applications.

Rapidly increasing population, economic development, and water contamination have resulted in unprecedented global fresh water demands.[1-3] To augment the freshwater supply and alleviate water scarcity, desalination of seawater and brackish water, which comprise 97.5% of the total water on earth,[4] has been extensively implemented by many countries in the past few decades.[5, 6] Over 19,000 water desalination plants have been built globally, reaching an estimated capacity of 100 million m^3/day by 2017.[7] Water desalination technologies include those without phase change processes, such as reverse osmosis (RO)[8-10] and electrodialysis (ED),[11, 12] and those that involve phase change processes, such as thermal distillation (i.e., boiling)[13, 14] and membrane distillation (MD).[15-17]

Membrane distillation, an advantageous thermally-driven membrane technology, generates clean water based on the vapor pressure difference between the two sides of a porous hydrophobic membrane.[18, 19] In direct contact membrane distillation (DCMD), the most common MD configuration, water evaporates on the hot feed water side of the membrane surface, diffuses across the microporous membrane, and condenses on the cold distillate side.[20, 21] MD can be operable under conditions with lower temperatures than boiling and lower pressures than RO,[22, 23] leading to decreased electricity input and less fouling or corrosion problems.[18] Moreover, less sophisticated equipment and pretreatment systems facilitate MD to possess small footprint, compactness, and high modularity.[18, 22-24] The use of renewable energy sources to heat feed saline water, such as waste heat from power plants[18, 25] and solar energy by implementing solar thermal collection systems,[26-30] further incentivizes MD's application for sustainable water desalination. However, one of the main challenges of conventional MD is temperature polarization, which results in a lowered surface temperature at the membrane-feed water interface with respect to its bulk water value.[21, 31, 32] Consequently, the cross-membrane

temperature difference is decreased, reducing the driving force for mass transport and undermining the overall MD performance.[33]

Most recently, light-driven localized heating at membrane surfaces that incorporate photothermal materials (e.g., Ag nanoparticles, carbon black, and nitrocellulose) has provided a means to alleviate the concerns brought by the influence of temperature polarization.[33-35] With the integration of photothermal materials, localized heating can be efficiently generated from incident light (especially, renewable solar irradiation), which helps to increase and maintain the membrane surface temperature at the membrane-feed water interface. The MD system using photothermal membranes can significantly reduce the electricity input, while possessing other advantages of conventional MD processes such as less fouling problems and the modularity to combine with other systems.[18] However, the photothermal materials demonstrated so far have several limitations which hinder their further development and commercial practicability. For example, Ag nanoparticles are prone to delamination or leakage from membranes into water.[33] The dissolution of photothermal material will restrict its utilization for certain MD configurations (e.g., vacuum membrane distillation), and also lead to the potential impairment of the membrane's photothermal performance during long term applications. On the other hand, the bilayer structure of carbon black coating on the membrane surface makes the carbon black membrane exhibit low photothermal conversion efficiency.[34] Besides, the synthesis methods of these composite membranes are often complex, involving phase inversion or electrospinning processes, which may be cost and energy intensive.

Herein, we demonstrate, for the first time, a simple, stable, and highly effective PDA coated polyvinylidene fluoride (PVDF) membrane for solar-driven membrane distillation. Polydopamine, as a mussel-inspired polymer,[36] has been extensively applied in surface

62 modifications owing to its inherent and robust adhesive properties and hydrophilic nature.[37]
63 Polydopamine can be easily coated on surfaces, regardless of their initial surface energy, making
64 the synthesis simple and cost-effective.[38] The PDA coating on organic substrates is extremely
65 stable under harsh conditions, including ultrasonication or acidic pH (<1), which makes the long-
66 term commercial application of PDA-coated materials viable.[36] Similar to those of naturally
67 occurring eumelanin,[39-43] PDA also exhibits broad light absorption and remarkable photothermal
68 conversion properties,[44, 45] which ensures its potential application for highly efficient solar-based
69 seawater desalination. Moreover, the biocompatibility,[46, 47] low toxicity and biodegradable nature
70 of PDA make it an environmentally benign material for water purification[41, 48] and biomedical
71 applications.[49, 50] Previously, PDA has been applied for seawater desalination techniques, such as
72 forward osmosis and nanofiltration, to increase the permeate flux facilitated by only exploiting
73 its hydrophilic nature.[51, 52] However, there is still plenty of room to utilize PDA for solar-driven
74 seawater desalination applications considering its superb photothermal properties, especially in
75 solar-driven membrane distillation. The solar-driven MD system using PDA in this study shows
76 the best thermal efficiency to date among currently reported photothermal MD systems, and the
77 highest water flux using a DCMD system among currently reported solar-driven MD studies.
78 The simple, stable, and highly effective photothermal membrane introduced in this study can
79 help to expand PDA's application and provide a promising option to alleviate the global fresh
80 water scarcity problems.

81 Polydopamine coating on a commercial hydrophilic PVDF membrane (0.45 μm pore size;
82 MilliporeSigma) can be easily achieved via a self-polymerization process (Fig. 1A and Fig. S1,
83 ESI†).[36, 39] The PVDF membrane has been widely used for MD systems,[19] and in our work,
84 hydrophilic PVDF was chosen to achieve easier and more efficient PDA coating owing to PDA's

85 hydrophilic nature. With 2 mg/mL dopamine (DA) in 10 mM Tris-HCl (pH 8.5) solution, the
86 self-polymerization process was repeated for 7 days to ensure that the entire surface of the PVDF
87 was uniformly coated by PDA (Fig. S1). The uniformity coating of PDA on PVDF surface can
88 minimize the influence of light illumination spot on the membrane's photothermal reactivity.
89 The amount of PDA coating can be tuned by varying the number of coating cycles, and the final
90 weight percentage of PDA on PVDF after 7 cycles was quantified to be 9.7±0.5 wt% by
91 measuring the weight difference of the membrane before and after polymerization. With the
92 additional coating of PDA, the porosity (ε) of the PDA-PVDF membrane decreased slightly
93 (73.2% ± 2.6%, compared with 82.1% ± 4.2% for a pristine PVDF membrane, measured by a
94 gravimetric method).[53-55] Hydrophobicity is important for MD membranes because it resists pore
95 wetting, ensures the passage of only the vapor phase through the membrane pores, and enhances
96 the salt rejection performance of the membrane.[20] The hydrophobicity of PDA-coated PVDF
97 membrane was increased by a facile fluoro-silanization method using (tridecafluoro-1,1,2,2-
98 tetrahydrooctyl)-trichlorosilane (FTCS),[56, 57] leading to a water contact angle of 125.5º. The
99 above processes are evident in a morphological investigation carried out by scanning electron
100 microscopy (SEM) and contact angle measurements, which clearly show a uniform and dense
101 coating of PDA on the microporous PVDF surface and cross-section (Fig. 1B-G), and the
102 successful hydrophobic modification of FTCS, respectively (inset in Fig. 1A). ImageJ analysis of
103 surface SEM images (×5000 magnification) indicates that an average surface pore size of FTCS-
104 PDA-PVDF membrane was 0.96 ± 0.42 μm by taking measurements of 100 pores.[58, 59] The
105 average pore size of FTCS-PDA-PVDF membrane became larger compared with pristine PVDF
106 membrane (0.46 ± 0.13 μm, confirmed by SEM images), which can be due to the fact that the
107 PDA coating closed the smaller pores rather than the bigger pores, making the average pore size

108 increase (Fig. 1B and 1E). Consequently, the pore numbers calculated from SEM images also
109 decreased from 2.6 $\times 10^7/cm^2$ of pristine PVDF membrane to $1.1\times 10^6/cm^2$ of FTCS-PDA-PVDF
110 membrane.

111 To further understand the chemical composition of the synthesized FTCS-PDA-PVDF
112 membrane, we have performed attenuated total reflection Fourier transform infrared (ATR-FTIR)
113 spectroscopy measurements (Fig. 2A). The characteristic N-H and C=C peaks of PDA on PVDF
114 at 1520 and 1610 cm^{-1},[60-63] and the Si-O peak of FTCS at 1010 cm^{-1},[64, 65] respectively indicated
115 the successful coating of PDA and the FTCS modification. The ATR-FTIR reference peaks for
116 PDA coating on PVDF are summarized in Table S1†. Raman spectroscopy also showed peaks of
117 PDA at 1350 and 1573 cm^{-1} (Fig. S2A†), corresponding to the stretching and deformation of
118 PDA's catechol groups.[66, 67] X-ray photoelectron spectroscopy (XPS) revealed the chemical
119 composition difference between pristine PVDF and FTCS-PDA-PVDF, based on the N 1s, Si 2p,
120 and C 1s peaks (Fig. 2B–D). As shown in Fig. 2B, a new N 1s peak emerged at 398–402 eV for
121 the FTCS-PDA-PVDF, corresponding to the N-C and N-H bonds of PDA layers on the surface
122 of PVDF membrane.[68] The new emerging Si 2p peak of FTCS-PDA-PVDF at 103.8 eV (Fig. 2C)
123 showed the Si-O bond of FTCS on the PDA-PVDF surface.[69] Within the broad C 1s peak (Fig.
124 2D), the increased relative ratio of $–CF_2–$ (290.2 eV) over $–CH_2–$ (285.2 eV) and the newly
125 appeared $–CF_3$ peak (292.3 eV) from FTCS-PDA-PVDF were attributed to the fluorinated tails
126 of FTCS on the PVDF surface.[70] Further, to evaluate the PDA coating effects on surface
127 roughness, the root-mean-square (RMS) roughnesses of both FTCS-PDA-PVDF (179 ± 12 nm)
128 and pristine PVDF (498 ± 31 nm) membranes were acquired by measuring tapping mode atomic
129 force microscopy (AFM) images (Fig. S2B†). The lowered surface roughness after PDA coating

130 can be attributed to the partial filling of large pores in the PVDF membrane with PDA, which
131 can also be observed in SEM images.

132 In light-to-heat conversion by photothermal materials, the light absorption properties are
133 of crucial importance. Hence, following the chemical characterization, the transmittance and
134 reflectance measurements of the FTCS-PDA-PVDF membrane were carried out in the range of
135 450–800 nm, using a micro-spectrophotometer (Fig. 3A and 3B, and the ESI†). The light
136 absorption properties of pristine PVDF membranes modified only by FTCS (FTCS-PVDF) and
137 by PDA (PDA-PVDF) were also measured for comparison. The FTCS-PVDF membrane showed
138 high transmittance (~17.1%) and reflectance (~27.6%) in the visible region, which indicated
139 relatively low light extinction (~55.3%). On the other hand, after PDA coating, the PDA-PVDF
140 and FTCS-PDA-PVDF membranes exhibited extremely small optical transmittance (~0.4% for
141 PDA-PVDF, and ~0.1% for FTCS-PDA-PVDF) and reflectance (~2.6% for PDA-PVDF, and
142 ~3.7% for FTCS-PDA-PVDF) in the visible region, indicating a large optical extinction (~97.0%
143 for PDA-PVDF, and ~96.2% for FTCS-PDA-PVDF) by the membrane. This excellent light
144 extinction property, which was mainly attributed to light absorption by the PDA coating and
145 light scattering by the membrane's porous structure,[37, 42] underlies the light-to-heat conversion of
146 the FTCS-PDA-PVDF membrane.

147 Further, to probe the photothermal conversion performance of the FTCS-PDA-PVDF
148 membrane, the surface temperatures of dry FTCS-PVDF, PDA-PVDF, and FTCS-PDA-PVDF
149 were measured by an infrared (IR) camera under light illumination from a solar simulator (Fig.
150 3C and 3D). Two light intensities were used to represent unfocused and focused illumination,
151 and the power densities were measured to be 0.75 (~0.7 sun) and 7.0 kW/m^2 (~7 sun)
152 respectively by a spectroradiometer (Fig. S3†). After 600 secs illumination, the surface

153 equilibrium temperature of dry FTCS-PDA-PVDF increased from room temperature (20 ºC) to
154 ~35 ºC (at 0.75 kW/m^2) and to ~97 ºC (at 7.0 kW/m^2). The surface temperature of the dry PDA-
155 PVDF membrane also increased from 20 ºC to ~35 ºC (0.75 kW/m^2) and to ~96 ºC (7.0 kW/m^2).
156 In comparison, the dry FTCS-PVDF membrane surface temperature increased only from 20 ºC to
157 ~23 ºC (0.75 kW/m^2) and to ~27 ºC (7.0 kW/m^2) under the same irradiation conditions. To
158 evaluate the photothermal conversion properties of the membranes under water, the surface
159 temperatures of membranes with water on top (8 mm distance from the membrane to the
160 air/water interface) were also monitored using a benchtop controller thermocouple probe. For
161 membranes immersed in water, the temperature increases on the top of the membrane surface
162 were smaller than those of dry membranes. Under water, after 600 sec illumination, the surface
163 equilibrium temperature of FTCS-PDA-PVDF membrane increased from 20 ºC to ~26 ºC (0.75
164 kW/m^2) and to ~32 ºC (7.0 kW/m^2), and the temperature of PDA-PVDF membrane increased
165 from 20 ºC to ~25 ºC (0.75 kW/m^2) and to ~31 ºC (7.0 kW/m^2), while the temperature of FTCS-
166 PVDF membrane increased only from 20 ºC to ~22 ºC (0.75 kW/m^2) and to ~24 ºC (7.0 kW/m^2).
167 The water on top of the membrane absorbed and scattered photons passing through, thus
168 reducing the number of photons absorbed by the PDA coating on the membrane. The above
169 results confirmed that the PDA coating on the PVDF surface exhibited high photothermal
170 conversion and can be utilized for localized heating under solar irradiation.

171 The solar-driven membrane distillation performance of the FTCS-PDA-PVDF membrane
172 was tested in a specially designed direct contact membrane distillation (DCMD) module (Fig. 4A
173 and Fig S4†). The distillate (DI water, 20 ºC) was circulated with a flow rate of 16.2 mL/min,
174 and the increasing weight of the distillate was measured continuously by a balance to quantify
175 the amount of collected water. To test the membrane distillation performance within 60 minutes

(Fig. 4B and 4C) under different salinities, both pure water and highly saline water (0.5 M NaCl) were used as feed water (20 ºC) with a flow rate of 3.6 mL/min. Here, the 0.5 M salinity was chosen to mimic the average salinity of seawater.[71] The FTCS-PVDF membrane was used as a control membrane for comparison. For the FTCS-PDA-PVDF membrane with pure water, the water flux was 0.58 $kg/m^2 \cdot h$ under 0.75 kW/m^2 irradiation. On the other hand, for the FTCS-PVDF membrane, the water flux was only 0.12 $kg/m^2 \cdot h$ under identical irradiation, which is 3.8 times lower than that of the FTCS-PDA-PVDF membrane. With higher irradiation intensity (7.0 kW/m^2), the water flux of the FTCS-PDA-PVDF membrane increased to 5.17 $kg/m^2 \cdot h$, 12.6 times higher than that of FTCS-PVDF membrane (0.38 $kg/m^2 \cdot h$) under identical irradiation. In comparison, the water flux collected with saline feed water was lower than that of pure water for both the FTCS-PVDF and FTCS-PDA-PVDF membranes. The water fluxes for the FTCS-PDA-PVDF membrane were 0.49 and 4.23 $kg/m^2 \cdot h$ under 0.75 and 7.0 kW/m^2 irradiations, significantly higher than those of the FTCS-PVDF membrane (0.09 and 0.22 $kg/m^2 \cdot h$). The lower water flux with saline water was due to the lower vapor pressure being in equilibrium with the feed, resulting in a lower vapor pressure difference across the membrane.[72, 73] To put the FTCS-PDA-PVDF membrane in real-world use perspective, with saline water, a permeate flux rate of ~0.49 $kg/m^2 \cdot h$, and an active area of $\sim 1 \times 1$ m^2, our solar MD system could generate 3.92 L/day under 0.75 kW/m^2 irradiation, with 8 h of sunlight time and at ~20 ºC ambient temperature. This outstanding solar-driven MD performance of the FTCS-PDA-PVDF membrane makes it highly attractive for efficient and sustainable desalination process.

The feed flow rate is crucial for MD efficiency because it affects the heat transfer in the feed channel and the temperature polarization effects on the membrane surface.[19] Therefore, to evaluate the influence of feed flow rate on the solar-driven MD performance, we also measured

199 the permeate water flux with varied feed flow rates (1.5–8.1 mL/min) for FTCS-PDA-PVDF
200 membranes (Fig. 4D, Fig. S5†) with simulated solar irradiation. The tests were conducted in
201 triplicate, using a new membrane each time. With 0.75 kW/m^2 irradiation, the fluxes with pure
202 water and saline water decreased from 0.66 and 0.57 kg/m^2·h to 0.49 and 0.43 kg/m^2·h,
203 respectively, when the feed flow rate increased from 1.5 to 8.1 mL/min. With 7.0 kW/m^2
204 irradiation, the fluxes with pure water and saline water decreased from 5.89 and 4.87 kg/m^2·h to
205 4.18 and 3.51 kg/m^2·h, respectively (Fig. S5A-B†). As shown in the schematic diagram
206 comparing conventional MD and solar-driven MD in Fig. S5C†, for conventional MD systems,
207 the permeate water flux increases with an increasing feed water flow rate, owing to better mixing
208 in the flow channel and decreased temperature polarization effects.[32, 74] Contrarily, in the solar-
209 driven MD system, the permeate water flux decreased with increasing feed water flow rate. With
210 higher feed flow rate, the heat loss from the heated membrane top surface to the bulk feed water
211 was faster, leading to a smaller temperature gradient across the membrane. Similar trends have
212 been reported in a recent study using carbon black as photothermal material.[34] However, with
213 feed flow rates of 1.5–8.1 mL/min and irradiation of 0.75 kW/m^2, the permeate flux with saline
214 feed water (0.5 M NaCl) of our membrane (0.43–0.57 kg/m^2·h) was about twice as high as that
215 reported for the carbon black membrane (~0.21–0.27 kg/m^2·h) under similar conditions.[34]

216 The solar conversion efficiency (η), which describes the overall membrane thermal
217 efficiency, was defined as the ratio of the energy needed to generate permeate flux over the total
218 energy input by solar irradiation (I, kJ/m^2·h) (same as the gained output ratio, see detailed
219 description in the section S4 in ESI†). The energy needed for permeate flux was calculated by
220 multiplying the permeate flux ($\dot{m}$, kg/m^2·h) by the evaporation enthalpy change (H_{vap}, 2,454
221 kJ/kg) of water.[34] As shown in Fig. 4E, with a pure water flow rate of 3.6 mL/min, the solar

222 conversion efficiency of the FTCS-PDA-PVDF membrane was calculated to be 53% under
223 0.75 kW/m^2 irradiation, much higher than the 10% of FTCS-PVDF under identical irradiation.
224 When the feed flow rates were adjusted from 1.5 to 8.1 mL/min, the solar efficiencies decreased
225 from 60% to 44%. At a flow rate of 3.6 mL/min with saline water, the solar conversion
226 efficiencies of FTCS-PDA-PVDF membranes were 45% and 41% under 0.75 and 7.0 kW/m^2
227 irradiations, respectively. For both pure water and saline water, the solar efficiencies decreased
228 when using larger feed flow rates. Previous studies have used silver nanoparticles, nitrocellulose,
229 and carbon black as photothermal materials for light-driven MD systems with excellent flux
230 penetration and solar conversion efficiencies.[33-35] However, our FTCS-PDA-PVDF membrane
231 exhibited even higher solar conversion efficiency (45% for saline water under 0.75 kW/m^2
232 irradiation) than membranes using silver nanoparticles (36.9%),[33] nitrocellulose (31.8%)[35] and
233 carbon black (21.5%)[34] (Table S2†). The outstanding solar conversion efficiency of the FTCS-
234 PDA-PVDF membrane compared with other recently reported membranes can be mainly
235 attributed to three factors: (i) The superior light absorption properties of PDA. Polydopamine has
236 wider light absorption range than Ag nanoparticles, which absorb light mainly in the UV range.[33]
237 (ii) The high surface temperature on the top of membrane owing to the excellent photothermal
238 conversion properties of PDA, even with a thick water layer on top of the membrane surface.
239 PDA is known to convert 99% of the absorbed photon energy into heat within 50 ps.[40] (iii) The
240 high density and uniformity of the PDA coating on the PVDF membrane surface as shown in
241 SEM images. The uniform self-polymerization of dopamine and the excellent adhesion of PDA
242 to a multitude of surfaces foster *'proximal'* photothermal conversion activity. Such proximal
243 photothermal conversion leads to an increased transmembrane temperature and a larger vapor
244 pressure difference across the membrane. In contrast, in the previous work using a carbon black

245 layer on top of the PVDF membrane, the light-absorbing layer is far from the PVDF membrane
246 surface, decreasing the transmembrane temperature and the driving force for vapor transport.[34]
247 In terms of solar conversion efficiency, although our membrane achieved the highest
248 efficiency among existing photothermal MD membranes, it is relatively lower than those of
249 photothermal steam generation membranes.[41, 75, 76] The main reasons behind the lower efficiency
250 in photothermal MD are the top water layer interference and conductive heat loss. With water
251 thickness ranging from 1.5–8 mm in existing photothermal MD systems (Table S2†), this top
252 water layer can reduce the number of photons absorbed by the photothermal membrane and thus
253 lead to a lower membrane surface temperature. In addition, the floating feed water system further
254 increases the conductive heat loss, while for photothermal steam generation, the untreated water
255 under the evaporators is often in a stagnant system. Although the efficiencies of current
256 photothermal steam generation are higher, the steam collection still remains as the challenge
257 before its large scale applications. In the future, efforts should be put into increasing the solar
258 conversion efficiency of photothermal MD by developing new MD modules or membranes to
259 exalt its competitiveness among all the photothermal desalination techniques. Furthermore,
260 photothermal MD can be more advantageous when it is used for flowback water treatment from
261 unconventional oil and gas recovery systems, which already contain high temperature water (e.g.,
262 ~60–70 ºC).[77] The high temperature feed water along with photothermal temperature rise, makes
263 the overall MD process more efficient.
264 The chemical and mechanical stability of the FTCS-PDA-PVDF membrane was
265 investigated further by subjecting it to both ultrasonic agitation for 6 hours and vigorous shaking
266 for 30 days at three pH values (pH 4, 7, and 10) (Fig. S6A†). Even after these extreme stress
267 tests, the FTCS-PDA-PVDF membrane did not exhibit discernible signs of disintegration or loss

268 of PDA coating from the surface. The morphology of the FTCS-PDA-PVDF membrane
269 remained unaltered after 10 cycling tests with pure water and saline water, as shown by the SEM
270 images of the FTCS-PDA-PVDF membrane surface (Fig. S6B-C†). Then, to evaluate the
271 potential changes in membrane wetting after several MD cycles, the contact angles of pure water
272 and saline water on the membrane were measured (Fig. S6D†). For an unused FTCS-PDA-
273 PVDF membrane, the contact angles were 125.5º ± 1.9º and 126.1º ± 1.6º for pure water and
274 saline water, respectively. After 10 cycles of MD tests (1 hr × 10 times), the contact angles for
275 pure water and saline water were 124.3º ± 1.5º and 125.4º ± 1.3º, indicating less than 1%
276 variation in the contact angle. Pore wetting problems have constrained the use of many MD
277 membranes for long term or large scale applications.[19] However, the excellent and stable
278 hydrophobicity of the FTCS-PDA-PVDF membrane, owing to the covalent and dense FTCS
279 fluoro-silane, confers long-lasting and stable wetting resistance. The variation of membrane mass
280 was also smaller than 1% over 10 cycles of MD tests using saline water with focused irradiation
281 (7.0 kW/m^2) (Fig. S6E†). The salt rejection was larger than 99.9% over 10 cycles of MD tests
282 using saline water under both unfocused (0.75 kW/m^2) and focused (7.0 kW/m^2) irradiations (Fig.
283 S6E†). This high salt rejection of FTCS-PDA-PVDF membrane can be attributed to the
284 operation conditions of the DCMD (low hydrostatic pressure), and to the excellent
285 hydrophobicity and wetting resistance of the membrane. Furthermore, the flux performance of
286 FTCS-PDA-PVDF membrane remained stable over 10 cycles of MD tests (less than 5%
287 variation, Fig. S6F†). The remarkable chemical and mechanical stability of the FTCS-PDA-
288 PVDF membrane, owing to the strong adhesion between PDA and the PVDF surface,[37, 60] can
289 lessen environmental concerns or the need for further treatment caused by the possible

detachment of photothermal materials from the membrane surface, and increase the longevity of membranes for long term solar MD applications.

In summary, we present a simple, stable, and highly effective photothermal membrane for solar-driven membrane distillation. Owing to the remarkable light absorption and outstanding photothermal conversion properties of the PDA coating, the FTCS-PDA-PVDF membrane exhibited excellent solar membrane distillation performance (efficiency of 45% under 0.75 kW/m^2 irradiation). The FTCS-PDA-PVDF membrane exhibited a 4.23 $kg/m^2 \cdot h$ permeate flux under 7.0 kW/m^2 irradiation, a 19-fold enhancement over FTCS-PVDF membrane. In addition, the proximal polymerization process that leads to strong adhesion between PDA and the PVDF surface resulted in the excellent chemical and mechanical robustness and stability of the FTCS-PDA-PVDF membrane, which allows its utilization in long term solar MD applications. In comparison with recently reported photothermal membranes which utilized phase inversion or electrospinning processes,[33, 34] PDA polymerization would be a much easier way to achieve proximal photothermal conversion activity. The simplicity of the PDA coating method also makes the membrane attractive for future commercial applications. From engineering perspectives, with built-up systems with multiple industrial-scale tanks, the final coated-membrane area can be significantly larger than other existing membrane modification methods to achieve a similar extent of photothermal performance. In the future, efforts can be put into expediting the PDA polymerization by optimizing the reaction conditions and designing better mixing systems. Coupled with renewable and sustainable solar irradiation, the highly efficient photothermal membrane introduced here can provide a promising option to alleviate the global water crisis.

Conflicts of interest

There are no conflicts to declare.

Acknowledgments

We are grateful for the support received from the National Science Foundation Environmental Engineering Program (CBET-1604542). We wish to thank the Institute of Materials Science and Engineering (IMSE) in Washington University in St. Louis for the use of XPS. We also thank the Nano Research Facility (NRF) at Washington University in St. Louis for use of SEM. We thank Mr. James Linders at Machine Shop of Department of Chemistry at Washington University in St. Louis for helping the design and building of MD module, and Prof. James Ballard for carefully reviewing our manuscript. Lastly, we also thank the Environmental NanoChemistry Group members for providing valuable discussions and suggestions for this paper.

324 **List of Figures**

325 **Fig. 1** (A) Schematic depicting the synthesis of the FTCS-PDA-PVDF membrane. SEM
326 images of the pristine PVDF membrane surface (B and C) and cross-section (D).
327 SEM images of the FTCS-PDA-PVDF membrane surface (E and F) and cross-
328 section (G).

329 **Fig. 2** Characterization of the FTCS-PDA-PVDF membrane. (A) ATR-FTIR spectra of the
330 pristine PVDF and the FTCS-PDA-PVDF membranes. XPS spectra of the pristine
331 PVDF and the FTCS-PDA-PVDF membranes showing the N 1s (B), Si 2p (C), and
332 C 1s (D) peaks.

333 **Fig. 3** Optical and thermal properties of the FTCS-PDA-PVDF membrane. (A)
334 Transmittance and (*inset*) reflectance spectra of the FTCS-PVDF, PDA-PVDF, and
335 FTCS-PDA-PVDF membranes. (B) Light extinction spectra of the FTCS-PVDF,
336 PDA-PVDF, and FTCS-PDA-PVDF membranes. (C) IR camera images of the
337 FTCS-PVDF membrane under illumination of 7.0 kW/m^2 (i), 0.75 kW/m^2 (iv), the
338 PDA-PVDF membrane under illumination of 7.0 kW/m^2 (ii), 0.75 kW/m^2 (v), and
339 the FTCS-PDA-PVDF membrane under 7.0 kW/m^2 (iii), and 0.75 kW/m^2 vi) after
340 600 sec illumination. (D) Surface temperature increase (ΔT, ºC) from room
341 temperature (20 ºC) of the FTCS-PVDF, PDA-PVDF, and FTCS-PDA-PVDF
342 membranes, after 600 sec illumination at 7.0 kW/m^2 and 0.75 kW/m^2, both under dry
343 conditions and under water (water thickness = 8 mm).

344 **Fig. 4** (A) Schematic depicting the solar-driven DCMD system. Collected water (kg/m^2)
345 using the FTCS-PVDF and the FTCS-PDA-PVDF membrane using both pure water
346 (B) and 0.5 M NaCl saline water (C) under different solar irradiations. Flux (D) and

efficiency (E) of solar-driven DCMD system using the FTCS-PDA-PVDF membrane with varying feed flow rates, using both pure water and 0.5 M NaCl saline water under different solar irradiations. Triplicate membrane samples were tested in all cases.

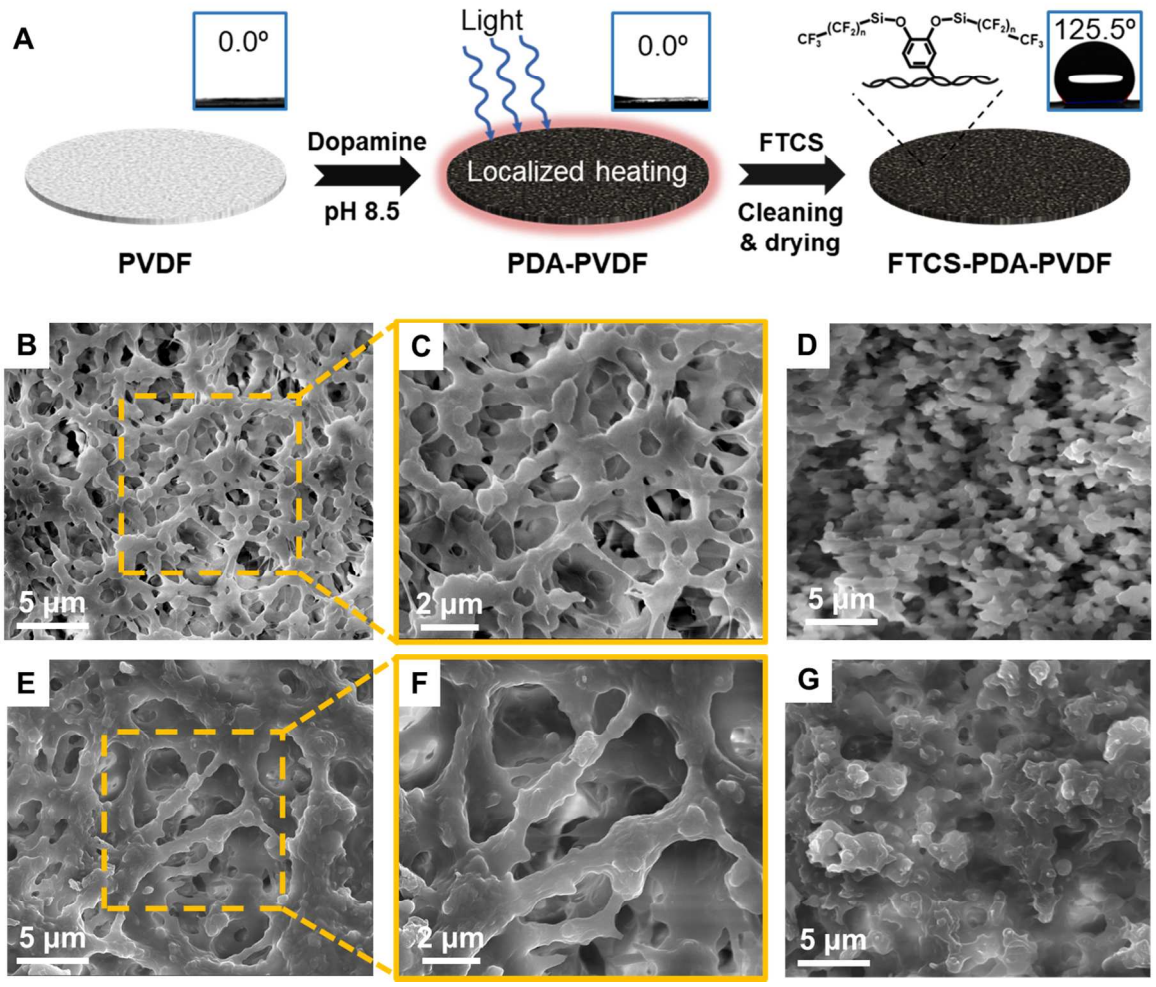
A
0.0°
Light
0.0°
125.5°
Dopamine
pH 8.5
Localized heating
FTCS
Cleaning
& drying
PVDF
PDA-PVDF
FTCS-PDA-PVDF
B
C
D
E
F
G
5 μm
2 μm
5 μm
5 μm
2 μm
5 μm

Fig. 1

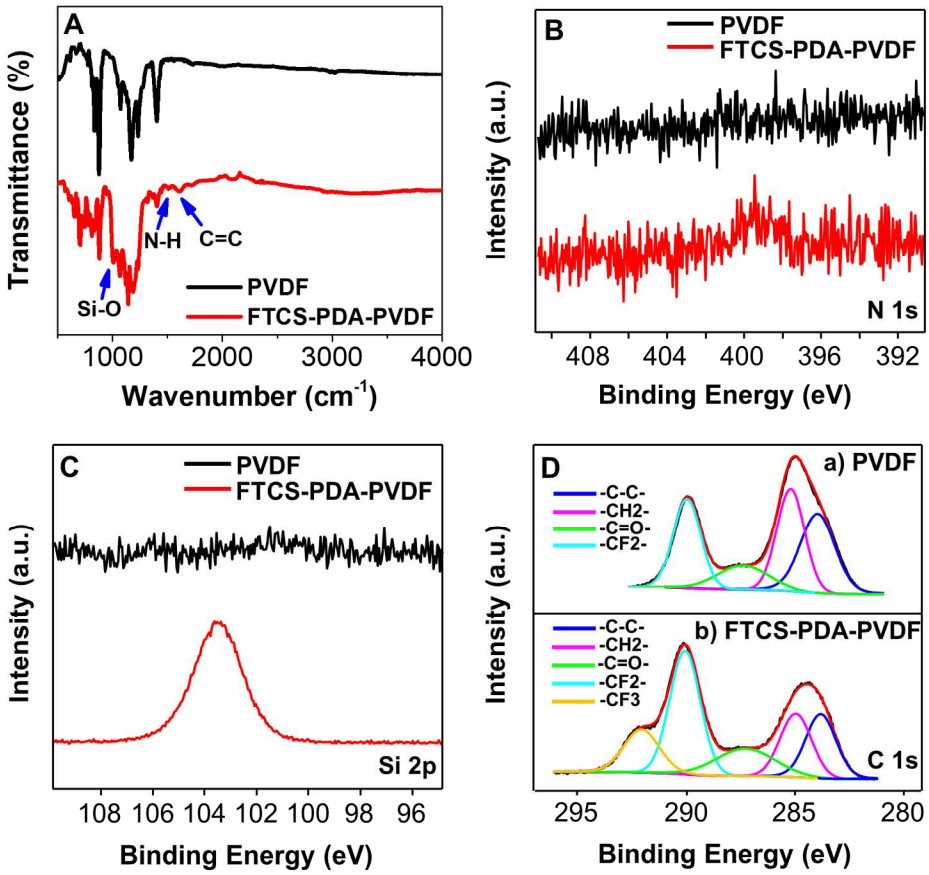
A
Transmittance (%)
N-H
C=C
Si-O
PVDF
FTCS-PDA-PVDF
1000
2000
3000
4000
Wavenumber (cm-1)
B
PVDF
FTCS-PDA-PVDF
Intensity (a.u.)
N 1s
408
404
400
396
392
Binding Energy (eV)
C
PVDF
FTCS-PDA-PVDF
Intensity (a.u.)
Si 2p
108
106
104
102
100
98
96
Binding Energy (eV)
D
a) PVDF
-C-C-
-CH2-
-C=O-
-CF2-
b) FTCS-PDA-PVDF
-C-C-
-CH2-
-C=O-
-CF2-
-CF3
Intensity (a.u.)
C 1s
295
290
285
280
Binding Energy (eV)

Fig. 2

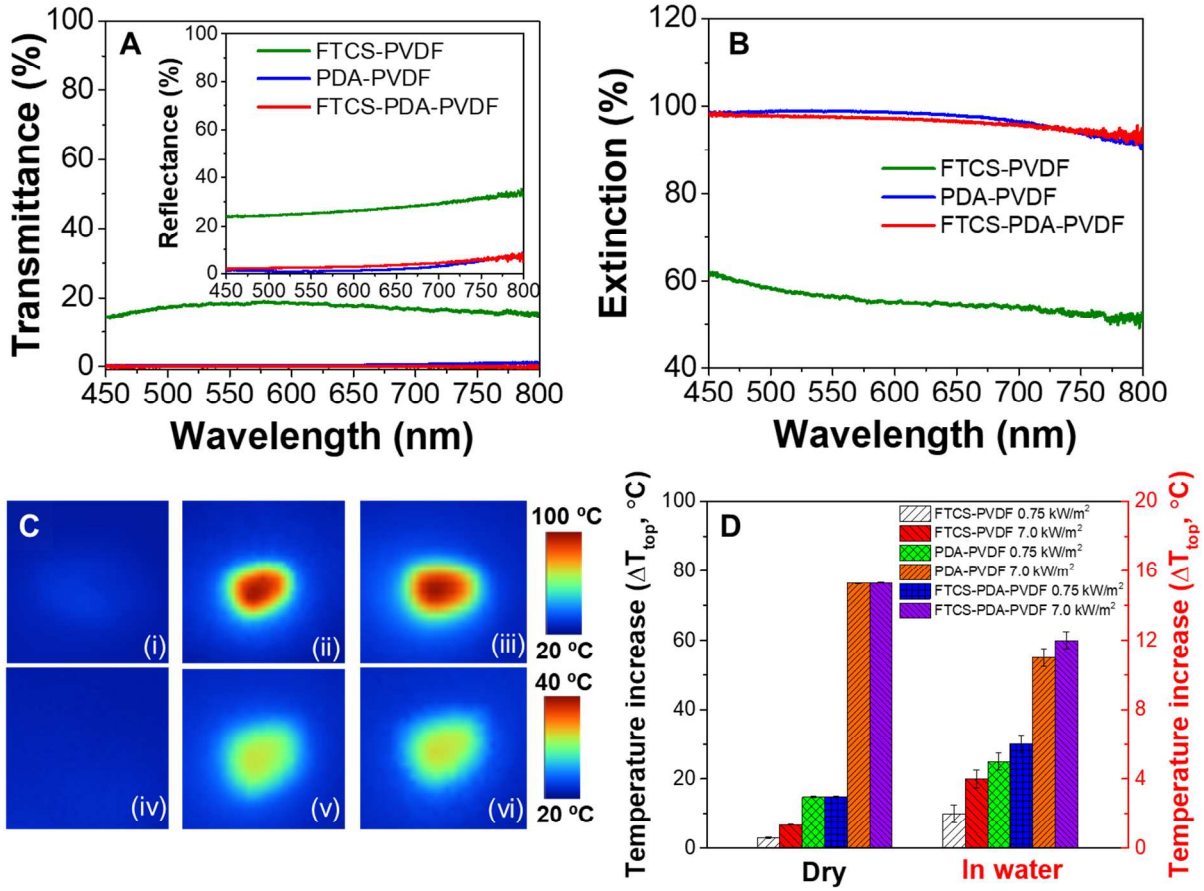
A
Transmittance (%)
Wavelength (nm)
Reflectance (%)
FTCS-PVDF
PDA-PVDF
FTCS-PDA-PVDF
B
Extinction (%)
Wavelength (nm)
FTCS-PVDF
PDA-PVDF
FTCS-PDA-PVDF
C
(i)
(ii)
(iii)
(iv)
(v)
(vi)
100 °C
20 °C
40 °C
20 °C
D
Temperature increase (ΔT_top, °C)
FTCS-PVDF 0.75 kW/m²
FTCS-PVDF 7.0 kW/m²
PDA-PVDF 0.75 kW/m²
PDA-PVDF 7.0 kW/m²
FTCS-PDA-PVDF 0.75 kW/m²
FTCS-PDA-PVDF 7.0 kW/m²
Dry
In water

Fig. 3

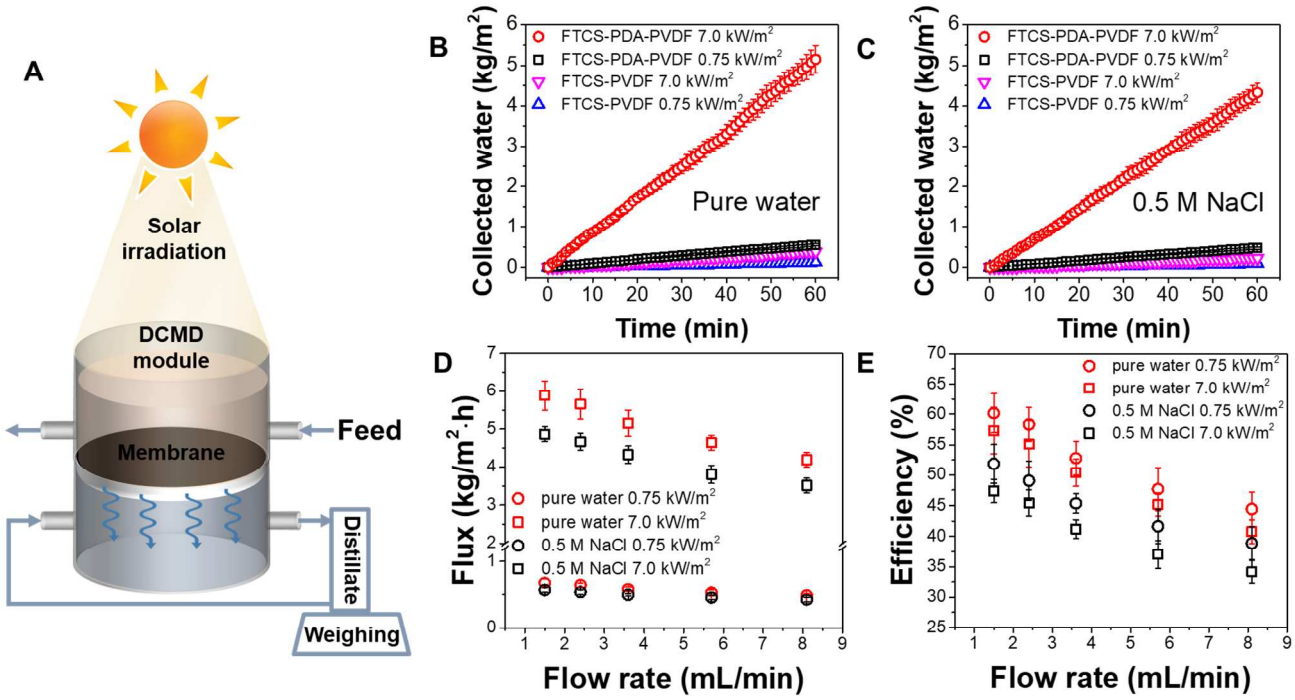
A
Solar irradiation
DCMD module
Membrane
Feed
Distillate
Weighing
B
Collected water (kg/m²)
FTCS-PDA-PVDF 7.0 kW/m²
FTCS-PDA-PVDF 0.75 kW/m²
FTCS-PVDF 7.0 kW/m²
FTCS-PVDF 0.75 kW/m²
Pure water
Time (min)
C
Collected water (kg/m²)
0.5 M NaCl
Time (min)
D
Flux (kg/m²·h)
pure water 0.75 kW/m²
pure water 7.0 kW/m²
0.5 M NaCl 0.75 kW/m²
0.5 M NaCl 7.0 kW/m²
Flow rate (mL/min)
E
Efficiency (%)
Flow rate (mL/min)

Fig. 4

References

1. J. Alcamo, M. Flörke and M. Märker, *Hydrolog. Sci. J.*, 2007, **52**, 247-275.
2. N. W. Arnell, *Glob. Environ. Change*, 2004, **14**, 31-52.
3. C. J. Vörösmarty, P. Green, J. Salisbury and R. B. Lammers, *Science*, 2000, **289**, 284-288.
4. H. T. El-Dessouky and H. M. Ettouney, *Fundamentals of salt water desalination*, Elsevier, 2002.
5. M. Elimelech and W. A. Phillip, *Science*, 2011, **333**, 712-717.
6. M. A. Shannon, P. W. Bohn, M. Elimelech, J. G. Georgiadis, B. J. Marinas and A. M. Mayes, *Nature*, 2008, **452**, 301.
7. IDA, *2016 – 2017 IDA Desalination Yearbook*, 2017.
8. A. E. Childress and M. Elimelech, *J. Membr. Sci.*, 1996, **119**, 253-268.
9. C. Fritzmann, J. Löwenberg, T. Wintgens and T. Melin, *Desalination*, 2007, **216**, 1-76.
10. L. F. Greenlee, D. F. Lawler, B. D. Freeman, B. Marrot and P. Moulin, *Water Res.*, 2009, **43**, 2317-2348.
11. J. Ortiz, J. Sotoca, E. Exposito, F. Gallud, V. Garcia-Garcia, V. Montiel and A. Aldaz, *J. Membr. Sci.*, 2005, **252**, 65-75.
12. M. Sadrzadeh and T. Mohammadi, *Desalination*, 2008, **221**, 440-447.
13. A. D. Khawaji, I. K. Kutubkhanah and J.-M. Wie, *Desalination*, 2008, **221**, 47-69.
14. D. Zhao, J. Xue, S. Li, H. Sun and Q.-d. Zhang, *Desalination*, 2011, **273**, 292-298.
15. A. Alkhudhiri, N. Darwish and N. Hilal, *Desalination*, 2012, **287**, 2-18.
16. K. W. Lawson and D. R. Lloyd, *J. Membr. Sci.*, 1997, **124**, 1-25.
17. M. K. Souhaimi and T. Matsuura, *Membrane distillation: principles and applications*, Elsevier, 2011.
18. A. Deshmukh, C. Boo, V. Karanikola, S. Lin, A. P. Straub, T. Tong, D. M. Warsinger and M. Elimelech, *Energy Environ. Sci.*, 2018.
19. M. El-Bourawi, Z. Ding, R. Ma and M. Khayet, *J. Membr. Sci.*, 2006, **285**, 4-29.
20. E. Drioli, A. Ali and F. Macedonio, *Desalination*, 2015, **356**, 56-84.
21. J. Phattaranawik, R. Jiraratananon and A. Fane, *J. Membr. Sci.*, 2003, **212**, 177-193.
22. L. M. Camacho, L. Dumée, J. Zhang, J.-d. Li, M. Duke, J. Gomez and S. Gray, *Water*, 2013, **5**, 94-196.
23. P. Goh, T. Matsuura, A. Ismail and N. Hilal, *Desalination*, 2016, **391**, 43-60.
24. A. Chafidz, S. Al-Zahrani, M. N. Al-Otaibi, C. F. Hoong, T. F. Lai and M. Prabu, *Desalination*, 2014, **345**, 36-49.
25. N. Dow, S. Gray, J. Zhang, E. Ostarcevic, A. Liubinas, P. Atherton, G. Roeszler, A. Gibbs and M. Duke, *Desalination*, 2016, **391**, 30-42.
26. T.-C. Chen and C.-D. Ho, *J. Membr. Sci.*, 2010, **358**, 122-130.
27. J. B. Gálvez, L. García-Rodríguez and I. Martín-Mateos, *Desalination*, 2009, **246**, 567-576.
28. P. Hogan, A. Fane and G. Morrison, *Desalination*, 1991, **81**, 81-90.
29. J. Koschikowski, M. Wieghaus and M. Rommel, *Desalination*, 2003, **156**, 295-304.
30. M. R. Qtaishat and F. Banat, *Desalination*, 2013, **308**, 186-197.
31. R. Schofield, A. Fane and C. Fell, *J. Membr. Sci.*, 1987, **33**, 299-313.
32. R. Schofield, A. Fane, C. Fell and R. Macoun, *Desalination*, 1990, **77**, 279-294.
33. A. Politano, P. Argurio, G. Di Profio, V. Sanna, A. Cupolillo, S. Chakraborty, H. A. Arafat and E. Curcio, *Adv. Mater.*, 2017, **29**.

34. P. D. Dongare, A. Alabastri, S. Pedersen, K. R. Zodrow, N. J. Hogan, O. Neumann, J. Wu, T. Wang, A. Deshmukh and M. Elimelech, *Proc. Natl. Acad. Sci.*, 2017, **114**, 6936-6941.
35. E. K. Summers, *Desalination*, 2013, **330**, 100-111.
36. H. Lee, S. M. Dellatore, W. M. Miller and P. B. Messersmith, *Science*, 2007, **318**, 426-430.
37. Y. Liu, K. Ai and L. Lu, *Chem. Rev.*, 2014, **114**, 5057-5115.
38. B. H. Kim, D. H. Lee, J. Y. Kim, D. O. Shin, H. Y. Jeong, S. Hong, J. M. Yun, C. M. Koo, H. Lee and S. O. Kim, *Adv. Mater.*, 2011, **23**, 5618-5622.
39. M. d'Ischia, A. Napolitano, V. Ball, C.-T. Chen and M. J. Buehler, *Acc. Chem. Res.*, 2014, **47**, 3541-3550.
40. S. E. Forest and J. D. Simon, *Photochem. Photobiol.*, 1998, **68**, 296-298.
41. Q. Jiang, H. G. Derami, D. Ghim, S. Cao, Y.-S. Jun and S. Singamaneni, *J. Mater. Chem. A*, 2017, **5**, 18397-18402.
42. J. Riesz, T. Sarna and P. Meredith, *J. Phys. Chem. B*, 2006, **110**, 13985-13990.
43. J. D. Simon, *Acc. Chem. Res.*, 2000, **33**, 307-313.
44. K. C. Black, J. Yi, J. G. Rivera, D. C. Zelasko-Leon and P. B. Messersmith, *Nanomedicine*, 2013, **8**, 17-28.
45. Y. Liu, K. Ai, J. Liu, M. Deng, Y. He and L. Lu, *Adv. Mater.*, 2013, **25**, 1353-1359.
46. S. Hong, K. Y. Kim, H. J. Wook, S. Y. Park, K. D. Lee, D. Y. Lee and H. Lee, *Nanomedicine*, 2011, **6**, 793-801.
47. S. H. Ku, J. Ryu, S. K. Hong, H. Lee and C. B. Park, *Biomaterials*, 2010, **31**, 2535-2541.
48. C. Zhang, M.-B. Wu, B.-H. Wu, J. Yang and Z.-K. Xu, *J. Mater. Chem. A*, 2018, **6**, 8880-8885.
49. M. Lee, J. Rho, D. E. Lee, S. Hong, S. J. Choi, P. B. Messersmith and H. Lee, *ChemPlusChem*, 2012, **77**, 987-990.
50. R. Mrówczyński, *ACS Appl. Mater. Inter.*, 2017, **10**, 7541-7561.
51. G. Han, S. Zhang, X. Li, N. Widjojo and T.-S. Chung, *Chem. Eng. Sci.*, 2012, **80**, 219-231.
52. G. Sun, T.-S. Chung, K. Jeyaseelan and A. Armugam, *Colloids Surf. B*, 2013, **102**, 466-471.
53. J. E. Efome, M. Baghbanzadeh, D. Rana, T. Matsuura and C. Q. Lan, *Desalination*, 2015, **373**, 47-57.
54. A. Khalifa, D. Lawal, M. Antar and M. Khayet, *Desalination*, 2015, **376**, 94-108.
55. U. Kuila, D. K. McCarty, A. Derkowski, T. B. Fischer and M. Prasad, *Fuel*, 2014, **117**, 1115-1129.
56. H. Jin, M. Kettunen, A. Laiho, H. Pynnönen, J. Paltakari, A. Marmur, O. Ikkala and R. H. Ras, *Langmuir*, 2011, **27**, 1930-1934.
57. M. E. Leitch, C. Li, O. Ikkala, M. S. Mauter and G. V. Lowry, *Environ. Sci. Technol. Lett.*, 2016, **3**, 85-91.
58. M. Sun, I. Zucker, D. M. Davenport, X. Zhou, J. Qu and M. Elimelech, *Environ. Sci. Technol.*, 2018.
59. A. Tiraferri, N. Y. Yip, W. A. Phillip, J. D. Schiffman and M. Elimelech, *J. Membr. Sci.*, 2011, **367**, 340-352.
60. C. Cao, L. Tan, W. Liu, J. Ma and L. Li, *J. Power Sources*, 2014, **248**, 224-229.
61. J. Jiang, L. Zhu, L. Zhu, B. Zhu and Y. Xu, *Langmuir*, 2011, **27**, 14180-14187.

62. L. Shao, Z. X. Wang, Y. L. Zhang, Z. X. Jiang and Y. Y. Liu, *J. Membr. Sci.*, 2014, **461**, 10-21.
63. D. Sun, Y. Zhu, M. Meng, Y. Qiao, Y. Yan and C. Li, *Sep. Purif. Technol.*, 2017, **175**, 19-26.
64. R. Al-Oweini and H. El-Rassy, *J. Mol. Struct*, 2009, **919**, 140-145.
65. P. Gupta, A. Dillon, A. Bracker and S. George, *Surf. Sci.*, 1991, **245**, 360-372.
66. G. Cheng and S.-Y. Zheng, *Sci Rep.*, 2014, **4**, 6947.
67. J. Ryu, S. H. Ku, H. Lee and C. B. Park, *Adv. Funct. Mater.*, 2010, **20**, 2132-2139.
68. J. Cui, Y. Zhang, Y. Wang, J. Ding, P. Yu, Y. Yan, C. Li and Z. Zhou, *New J. Chem.*, 2018, **42**, 118-128.
69. Y. Wu, J. Lu, M. Meng, J. Dai, X. Lin, J. Gao, C. Li and Y. Yan, *Chem. Eng. J.*, 2017, **309**, 263-271.
70. L.-F. Ren, F. Xia, V. Chen, J. Shao, R. Chen and Y. He, *Desalination*, 2017, **423**, 1-11.
71. H. A. Loáiciga, *Geophys. Res. Lett.*, 2006, **33**.
72. L. Martínez-Díez and M. I. Vazquez-Gonzalez, *J. Membr. Sci.*, 1999, **156**, 265-273.
73. D. Winter, J. Koschikowski and M. Wieghaus, *J. Membr. Sci.*, 2011, **375**, 104-112.
74. T. Y. Cath, V. D. Adams and A. E. Childress, *J. Membr. Sci.*, 2004, **228**, 5-16.
75. C. Chen, Y. Li, J. Song, Z. Yang, Y. Kuang, E. Hitz, C. Jia, A. Gong, F. Jiang, J. Zhu, B. Yang, J. Xie and L. Hu, *Adv. Mater.*, 2017, **29**, 1701756.
76. X. Hu, W. Xu, L. Zhou, Y. Tan, Y. Wang, S. Zhu and J. Zhu, *Adv. Mater.*, 2017, **29**, 1604031.
77. H. R. Acharya, C. Henderson, H. Matis, H. Kommepalli, B. Moore and H. Wang, *DOE Report DE-FE0000784*, 2011, 100.

Table of contents entry:

This study demonstrates a simple, stable, and scalable polydopamine (PDA) coated PVDF membrane for highly efficient solar-driven membrane distillation.